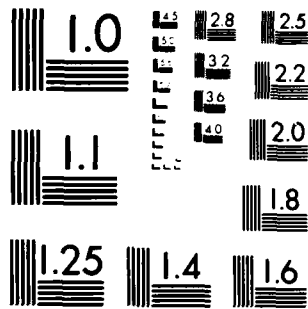MICROCOPY RESOLUTION TEST CHART

NATIONAL BUREAU OF STANDARDS-1963-A

PHYSICAL MODELING TECHNIQUES FOR MISSILE
AND OTHER
PROTECTIVE STRUCTURES

Papers Submitted for Presentation During the
American Society of Civil Engineers
National Spring Convention
Las Vegas, April 1982

Sponsored By the ASCE Engineering Mechanics Division
Committee on Experimental Analysis and Instrumentation

Edited By: T. Krauthammer and C. D. Sutton

83 02 02 004

TO
PA   29 Jun 83

ECT   Review of Material for Public Release

TO   Mr. James Shafer
        Defense Technical Information Center
        DDAC
   Cameron Station
        Alexandria, VA 22314

The following technical papers have been reviewed by our office and are
approved for public release. This headquarters has no objection to their
public release and authorizes publication.

1. (BMO 81-296) "Protective Vertical Shelters" by Ian Narain, A.M. ASCE,
Jerry Stepheno, A.M. ASCE, and Gary Landon, A.M. ASCE.

2. (BMO 82-020) "Dynamic Cylinder Test Program" by Jerry Stephens, A.M.
ASCE.

3. (AFCMD/82-018) "Blast and Shock Field Test Management" by Michael
Noble.

4. (AFCMD/82-014) "A Comparison of Nuclear Simulation Techniques on
Generic MX Structures" by John Betz.

5. (AFCMD/82-013) "Finite Element Dynamic Analysis of the DCT-2 Models"
by Barry Bingham.

6. (AFCMD/82-017) "MX Basing Development Derived From H. E. Testing" by
Donald Cole.

7. (BMO 82-017) "Testing of Reduced-Scale Concrete MX-Shelters-
Experimental Program" by J. I. Daniel and D. M. Schultz.

8. (BMO 82-017) "Testing of Reduced-Scale Concrete MX-Shelters-Specimen
Construction" by A. T. Ciolko.

9. (BMO 82-017) "Testing of Reduced-Scale Concrete MX-Shelters-
Instrumentation and Load Control" by N. W. Hanson and J. T. Julien.

10. (BMO 82-003) "Laboratory Investigation of Expansion, Venting, and
Shock Attenuation in the MX Trench" by J. K. Gran, J. R. Bruce, and J. D.
Colton.

11. (BMO 82-003) "Small-Scale Tests of MX Vertical Shelter Structures" by J. K. Gran, J. R. Bruce, and J. D. Colton.

12. (BMO 82-001) "Determination of Soil Properties Through Ground Motion Analysis" by John Frye and Norman Lipner.

13. (BMO 82-062) "Instrumentation for Protective Structures Testing" by Joe Quintana.

14. (BMO 82-105) "1/5 Size VHS Series Blast and Shock Simulations" by Michael Noble.

15. (BMO 82-126) "The Use of Physical Models in Development of the MX Protective Shelter" by Eugene Sevin.

*16. REJECTED: (BMO 82-029) "Survey of Experimental Work on the Dynamic Behavior of Concrete Structures in the USSR" by Leonid Millstein and Gajanen Sabnis.

CAROL A. SCHALKHAM, 1Lt, USAF
Public Affairs Officer

Cy To: Dr. T. Krauthammer
        Associate Professor
        Department of Civil and
        Mineral Engineering
        University of Minnesota
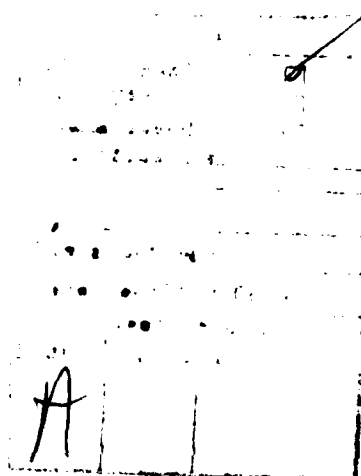
A COMPARISON OF NUCLEAR SIMULATION TECHNIQUES ON GENERIC MX STRUCTURES

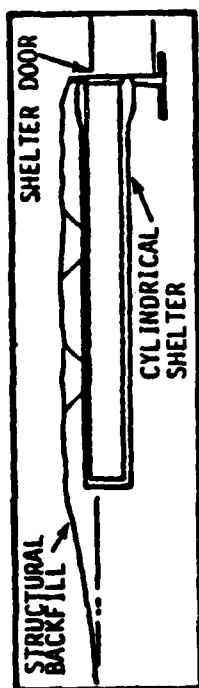By John F. Betz[1]

INTRODUCTION.

Land based MX missiles represent an important system in the offensive triad of the United States military strategy. Deployment of this new weapon system in a shallow-buried horizontal configuration created the need for a missile shelter design which could ensure survivability. Structural designs had to be accomplished starting with simplified techniques and proceeding with testing and advanced computer analysis. Once a generic MX protective structure had been developed to a stage nearing completion, large scale testing of the structure under anticipated attack scenarios began.

Two main nonnuclear simulation techniques which are used to reproduce nuclear airblast pressure loading were considered for use at large scale (1/5 scale up to full scale). These are the Dynamic Airblast Simulator (DABS) and the High Explosive Simulation Technique (HEST). The DABS is a high quality simulator which reproduces both static and dynamic airblast pressure loadings. The DABS configuration for the 1/5 scale test on the generic protective structure is shown in Figure 1. The simulator is essentially a semicircular cylinder with an explosive driver on one end and a free surface on the other end, with the test structure located at the desired range in between. The results from the DABS pressure loading in that 1/5 scale test were used to design the HEST layout for the follow-on test. Shown in Figure 2, the HEST was designed with eight different zones to duplicate the DABS loading on and around the generic structure.

Although each test revealed much about the structural response and survivability of the protective structure, the reason both tests were performed was to see if the HEST could perform as well as the DABS in simulating nuclear blast pressure loading. Cost was a driving force

---
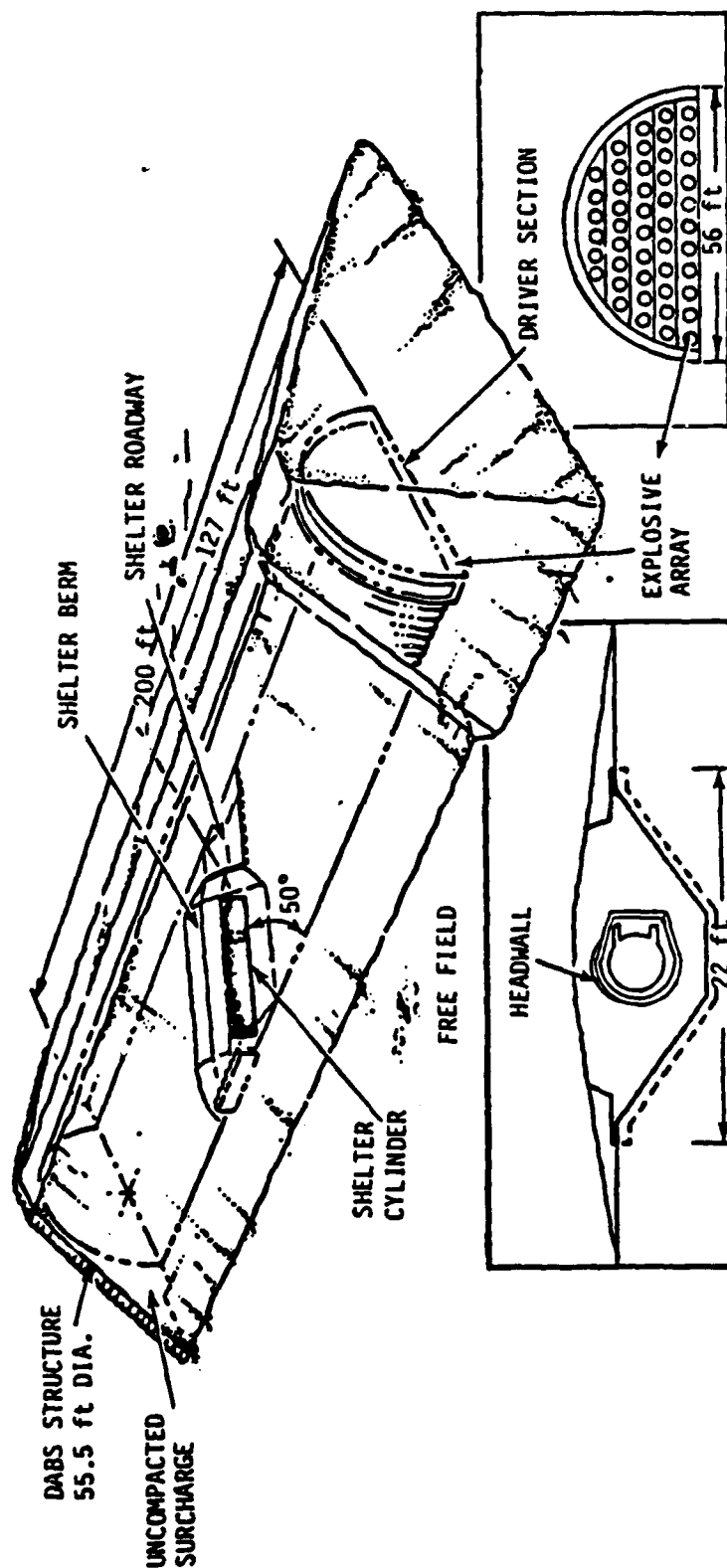
Figure 1. DABS layout for 1/5 scale D-1 test.

SHELTER DOOR

SHELTER BERM

SHELTER ROADWAY

127 ft

~200 ft

1 ft = 0.3048 m

STRUCTURAL BACKFILL

CYLINDRICAL SHELTER

DABS STRUCTURE 55.5 ft DIA.

UNCOMPACTED SURCHARGE

50°

SHELTER CYLINDER

FREE FIELD

HEADWALL

22 ft

DRIVER SECTION

56 ft

EXPLOSIVE ARRAY

2

ZONE 8-1
(3)

ZONE 5
(4.2)

ZONE 4
(6/28)

ZONE 6
(3)

ZONE 8-2
(3)

ZONE 1
(2.5)

ZONE 2
(8)

ZONE 3
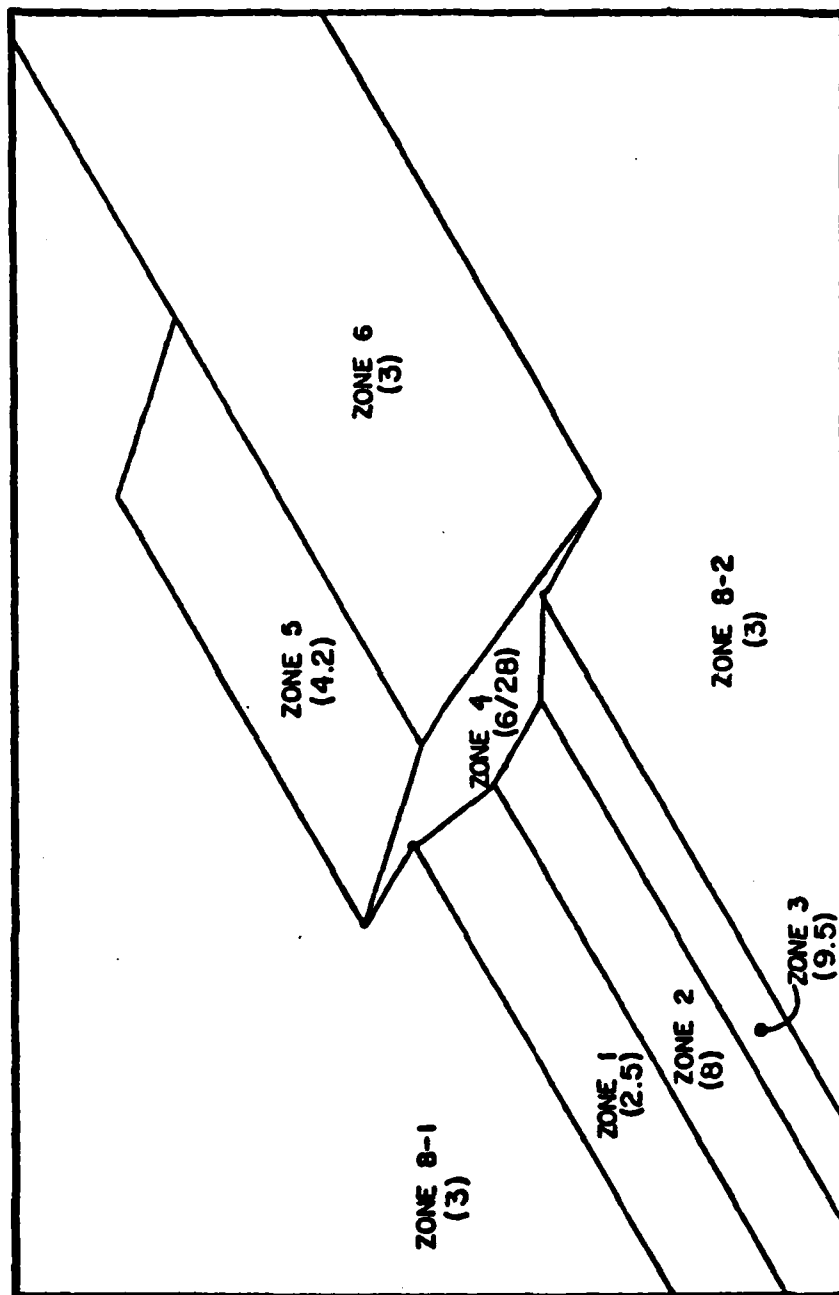(9.5)

( ) PRESSURE IN MPa
1 MPa = 145 psi

Figure 2. HEST configuration for 1/5 scale test (SH-1) based on DABS pressures.

3

behind this evaluation, because for tests 1/5 scale and larger, DABS simulation is at least twice as expensive as HEST simulation. Therefore, using the generic model response as a yardstick, the HEST simulation was measured against the DABS standard.

SURFACE PRESSURES.

Overall, the SH-1 (HEST test) and D-1 (DABS test) airblast pressure loading were very similar in magnitude, waveform and timing. Peak pressure loading of the front of the structure and the surrounding headwall was 20 to 50 percent higher than D-1 for SH-1. Impulse loading is also around 20 percent higher than D-1 along the face of the structure.

Airblast pressure loading on the berm and berm sides atop the structure had higher peak magnitudes and impulse loadings in SH-1 than D-1. As was the case for the headwall loading, the peak pressures and the impulse were 20 to 50 percent higher for SH-1 than for D-1.

An examination of the near field soil stresses and velocities indicated the same trend shown in the airblast pressure data. While the near field soil gages had more variation than the blast pressure readings, the data for SH-1 tended to be 25 to 100 percent greater in peak magnitude than for D-1. The timing and shape of the soil near field waveforms, like the airblast pressure waveforms, were very closely matched between the two simulations.

With the airblast pressure data and soil near field data indicating that the two tests had very similar simulations, structural response parameters from D-1 and SH-1 should match quite well with SH-1 data magnitudes generally greater than D-1 magnitudes.

STRUCTURAL RESPONSE.

In evaluating the similarity between the structural loads and response between SH-1 and D-1, data from three main sources were used. First of all, normal stress at the soil-structure interface provided a comparison of the normal stress on the structure through the soil. Then, velocity and integrated acceleration data showed how well structural motions matched between the tests. Finally, strain data indicated the modes of response and their relative severity in both D-1 and SH-1.

Before examining the specific structural data, however, some general understanding of the comparison would help clarify the data which will be presented. Neither the D-1 nor the SH-1 test exhibited any signs of severe plastic behavior. There was minor hairline tensile cracking in each test due to ovaling and due to other deformations under loads. Generally, structural response indicates initial response due to direct airblast loading only, then the response is affected more and more by normal stress and shear stress loading of the structure. Vertical longitudinal bending of the structure occurred in both tests, as did two distinct cycles of positive ovaling response (crown and invert move closer). Although the responses of both tests matched well overall, the position of maximum response was not always the same. For example, the location of the maximum vertical longitudinal bending moment was farther aft in SH-1 than D-1 due to the greater magnitude of SH-1 airblast pressure loading of the headwall, which caused the effective support of the front of the structure to extend farther aft. Overall, D-1 and SH-1 waveforms and timing matched very nicely, but the magnitudes of the response in SH-1 were 50 to 100 percent greater on the average.

SMI CHARACTERIZATION.

Structure-Media Interaction (SMI) loading on the structure provides the second major loading transmitter to the structure (direct airblast loading is the other one). While direct airblast loading causes the most immediate response of the structure, airblast-induced ground shock generates structural response in concert with the remaining direct airblast loading of the structure after the primary compressive wave effects. This is seen in both tests in the longitudinal response of the structure, which consists of two distinct peaks: the first due to direct airblast loading, and the second due to reflected airblast loading and soil drag-back shear stress occurring in the frontal region of the structure. Separating the two peaks (seen in both longitudinal velocity and strain data) is a relief caused by the normal stress induced by airblast loading of the berm atop the structure propagating along the structure and "gripping" the structure.

As seen in Figure 3, the normal stress at the crown, spring-lines, and invert at the region just behind the headwall agrees overall
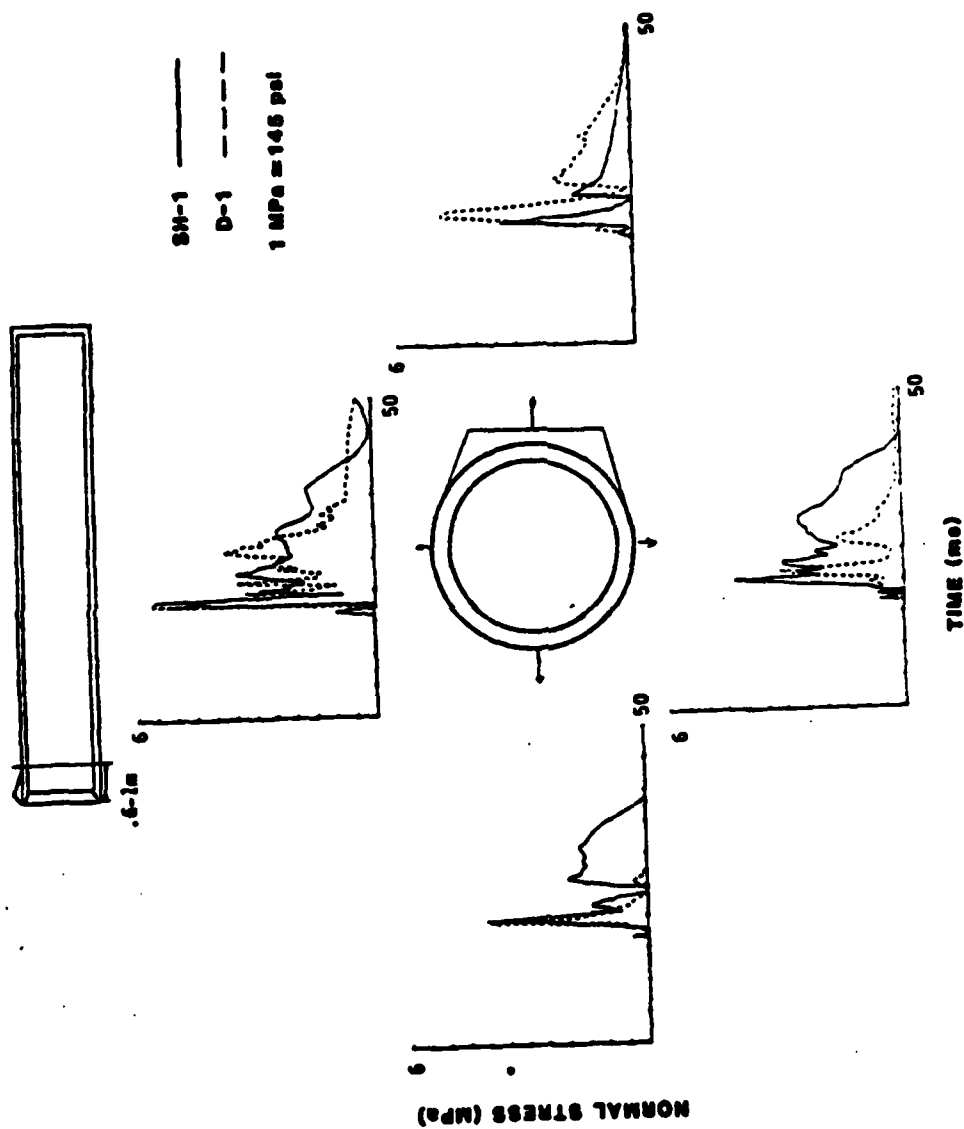
5

Figure 3. Forward normal stress.

6

in timing and waveform with the normal stress tracings from corresponding locations in D-1. The magnitudes are slightly higher for SH-1, as seen at the upstream springline and invert. However, the waveform does not seem similar at the invert, and the D-1 normal stress magnitudes are higher at the downstream springline. First of all, when the structure is placed at the test site, it rests in a 120° cradle of sand. Good contact between the invert gage and the surrounding media is not controllable in those conditions. Therefore, those gage readings are not always the best, and that variation seen at the invert is not beyond reasonable agreement for two tests. Second of all, the reading at the downstream springline, while showing a greater D-1 normal stress, shows very good agreement in the waveforms. Once again, the variation in the waveforms could be due to placement problems with the soil against the gage for SH-1. Regardless of that, the variation is not beyond that which can be seen in a single test alone.

Figure 4, which illustrates the normal stresses at the rear of the structure, shows the D-1 normal stresses to be higher across the section. The overall agreements are good for magnitudes and waveforms, except at the upstream springline, where the SH-1 normal stress data must have a problem with the scale but the waveforms are quite similar in peak timing and shape. SH-1 berm loading was not as high at the aft end of the structure as in the more forward regions, so that could be a partial explanation for the lower magnitude of SH-1 normal stresses.

Higher frontal loading in SH-1 causes higher longitudinal soil velocities which are reflected in part in both the longitudinal shear stress and the longitudinal structural velocity. SH-1 had greater drag-back shear stress magnitudes and a greater portion of the length which this drag-back shear acted upon than D-1. This, in turn, is reflected in the second longitudinal velocity peak and the secondary compressive strain pulse, although the separation of effects between initial airblast loading and later shear stress and reflected airblast loading grows less distinct toward the end wall.

SMI effects, then, are similar in comparison with the airblast pressure and the near field parameters already investigated. SH-1 mimics D-1 very closely in SMI behavior, but generally the magnitudes in SH-1 are greater due to the greater loading in the simulation.
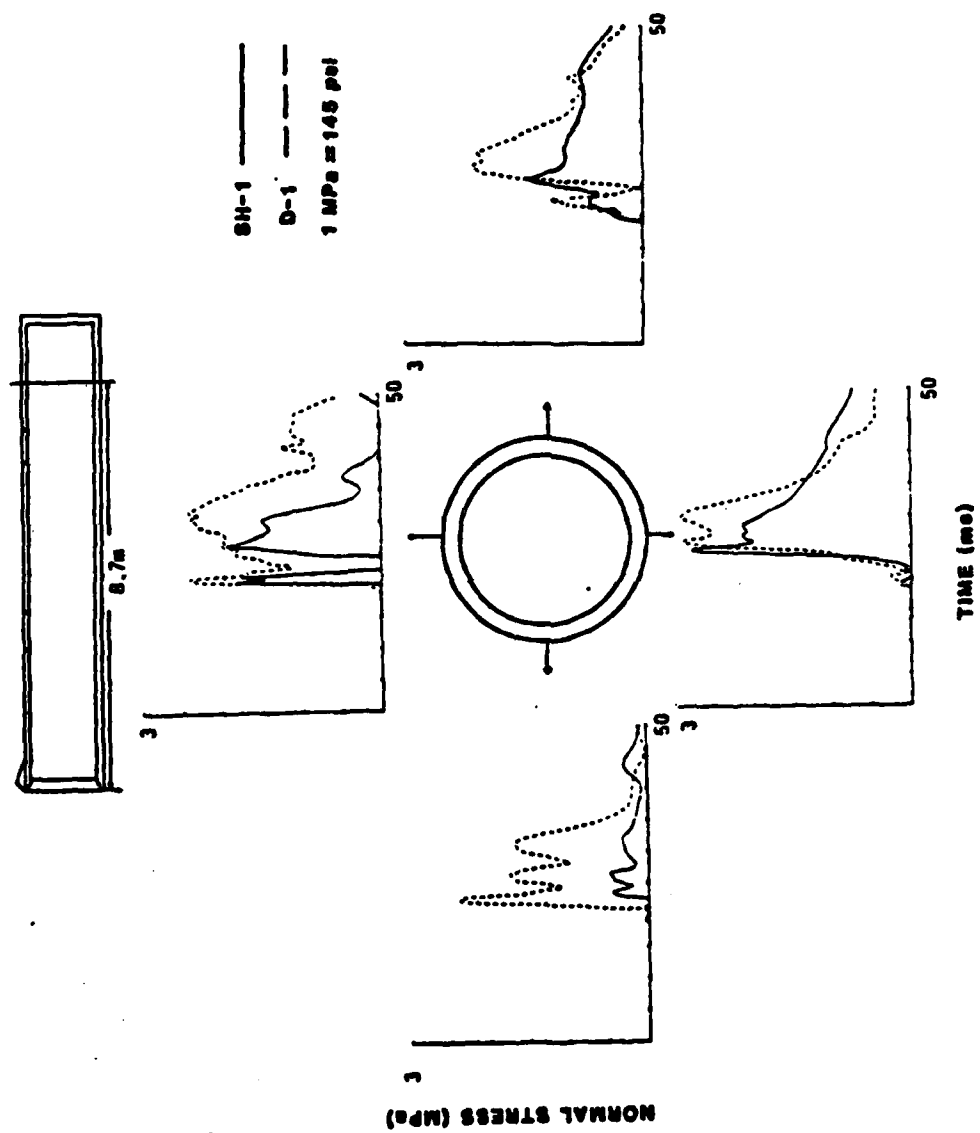
7

Figure 4. Aft normal stress.

8

VELOCITY CHARACTERIZATION.

Structural velocities are useful in examining the movement response of the structure under the loading caused by the attack scenario. The overall waveforms are usually easy to explain, especially in light of the loading conditions already explored.

Structural longitudinal velocities are presented in Figure 5. As already explained, they consist mainly of a double peak positive waveform with a relief seen in-between. The initial velocity peak is due to the direct airblast loading on the face of the structure. Normal stress application caused by vertical airblast-induced ground shock accounts for the slowing in-between peaks, while the second longitudinal velocity peak is due to both secondary airblast peaks loading the structure face directly and positive "drag-back" shear stress acting in the frontal third of the structure. As shown in Figure 5, the structural longitudinal velocities are greater in SH-1 than in D-1 due to the slightly higher airblast loading. Near coincidence of the peaks in the aft of the structure accounts for the higher velocity magnitudes.

The vertical structural velocity profile is given in Figure 6. This waveform is characterized by an initial high peak due to incident normal stress from vertical airblast-induced ground shock, with a usually minor second peak as the ground shock envelops the cross-section and a rigid-body vertical displacement occurs. Once again, the waveforms agree between D-1 and SH-1, with greater magnitudes seen in SH-1 due to the greater airblast loads on the berm. The forward velocity readings for this profile are more rounded because of the type of gage used to record the data.

The lateral structural velocities are shown in Figure 7. The best agreement is seen at the rear of the structure when comparing D-1 and SH-1. The expected velocity waveform for lateral velocities is shown consistently in D-1 data, where the crown of the structure displaces downstream, followed by the invert when the vertically-propagating ground shock arrives there. SH-1 showed consistently negligible lateral movement in the forward half of the structure. This could be due in part to the higher downstream stresses caused by greater airblast loading acting to restrain lateral motion.
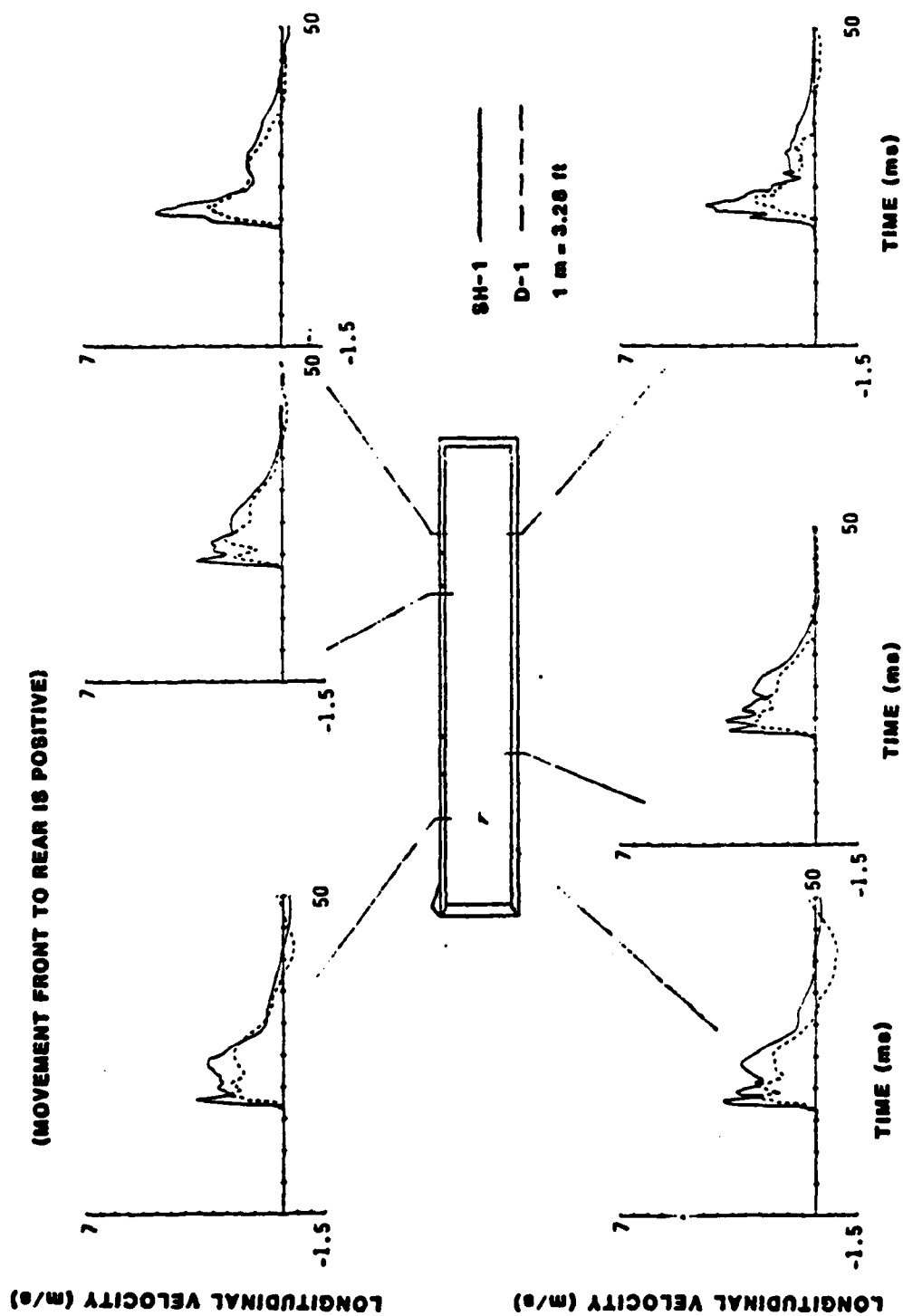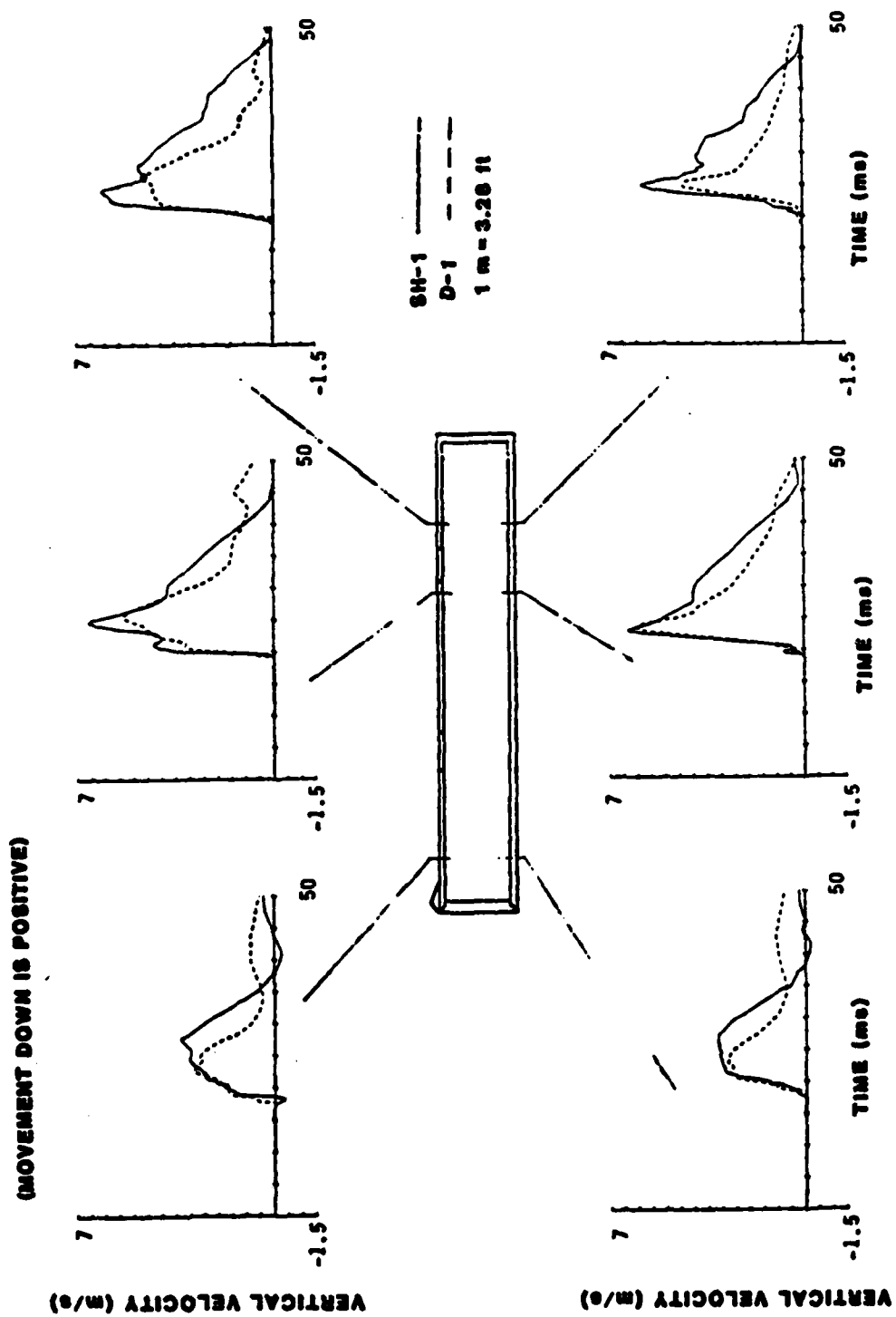
Figure 5. Structural longitudinal velocities.
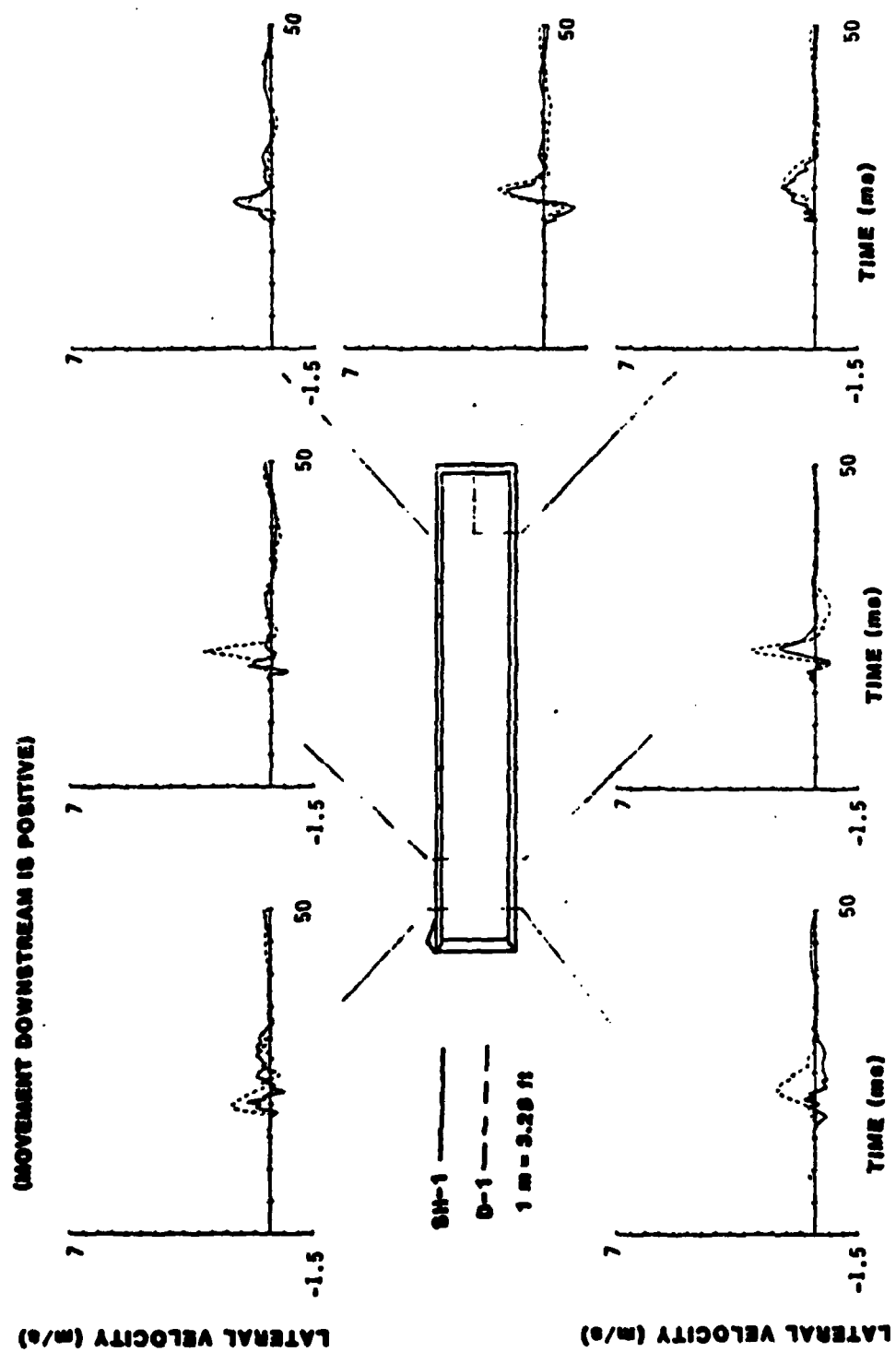
Figure 6. Structural vertical velocities.

11

Figure 7. Structural lateral velocities.

12

Taking an overview of the velocity-profiles shows that the vertical structural velocities were of greatest magnitude, followed closely by the longitudinal structural velocities. Both the vertical and longitudinal velocities agreed with the D-1 waveforms but had higher magnitudes. The SH-1 lateral structural velocities were consistently lower than D-1 except in the aft third of the structure, where the waveforms and magnitudes matched well for the two tests. Agreement of the velocity data between the two tests is surprisingly close, given the difference in blast simulators and the higher SH-1 loading. Indications are that similar structural responses occurred in both tests, since no noteworthy variations were seen in the velocity comparisons for the two tests. An investigation of the strain data will be the final measure of the capability of a HEST simulator to reproduce a DABS blast loading of a test structure.

STRAIN CHARACTERIZATION.

Structural strain data from the D-1 and SH-1 tests gave the best indications of structural response, especially in light of the loading conditions and the velocity response of each test. A great number of strain gages were placed in the structure at specific regions so that response could be defined in a more detailed manner. Representative cases will be used for this comparison between SH-1 and D-1 strain data. Cases will be examined in cross-sections from the front to the rear of the structure.

Strain near the supported edge of the closure base pan is presented in Figure 8. Tensile strain is expected in the data from the vertically-oriented gage, and both D-1 and SH-1 reflect this condition as the closure dishes inward under the airblast load. The waveforms reflect the higher SH-1 loading, but the timing of the three peaks in both tests coincide regardless of the airblast loading differences. This is because the peaks reflect the closure frequency of 500 Hz, which should agree in both tests with the same closure design.

Longitudinal strains at a section 2 meters from the front of the structure are seen in Figure 9. Inner and outer strains for both tests are shown at the crown and upstream springline, while only outer longitudinal strains are shown at the invert and downstream springline.
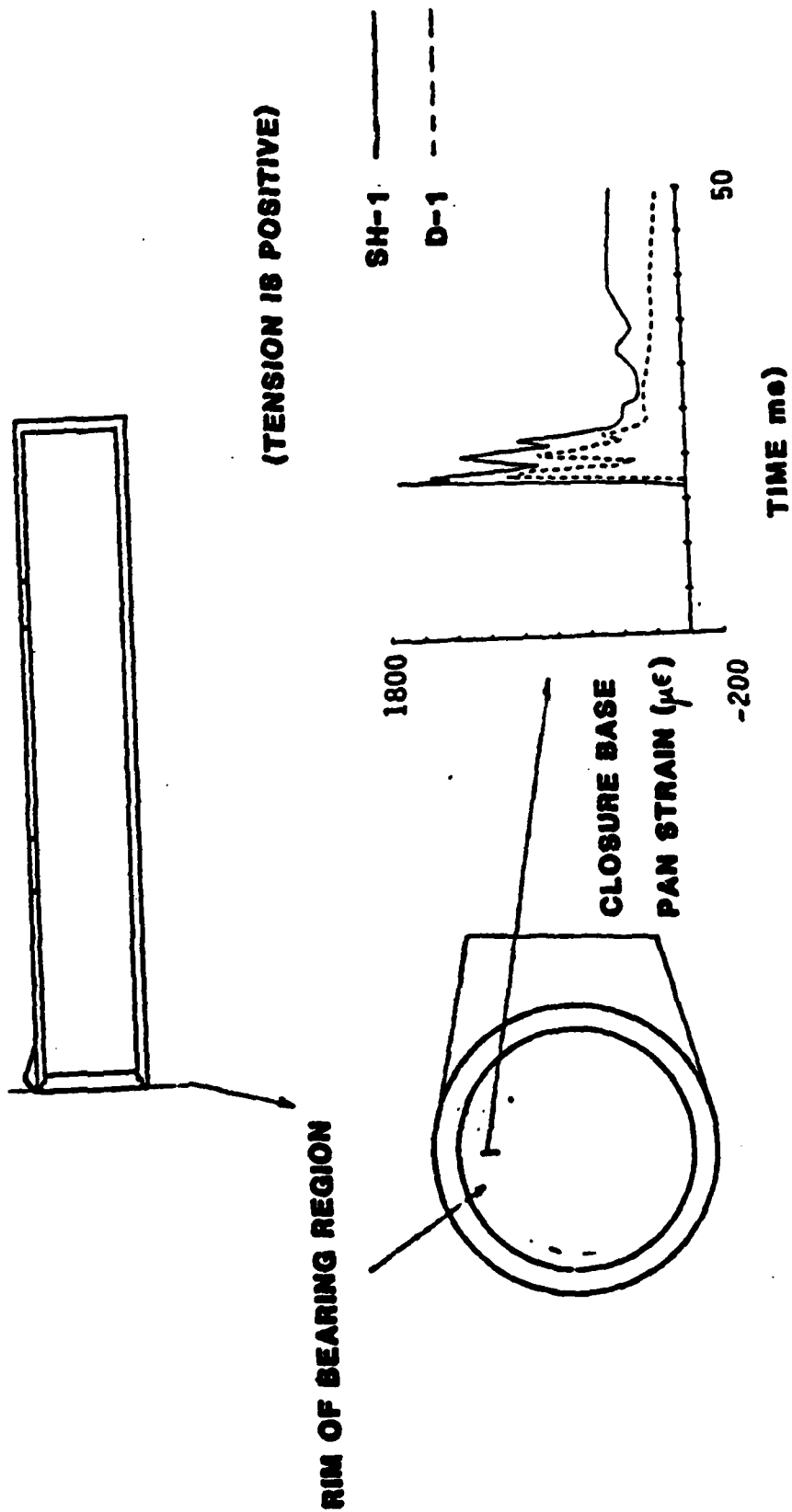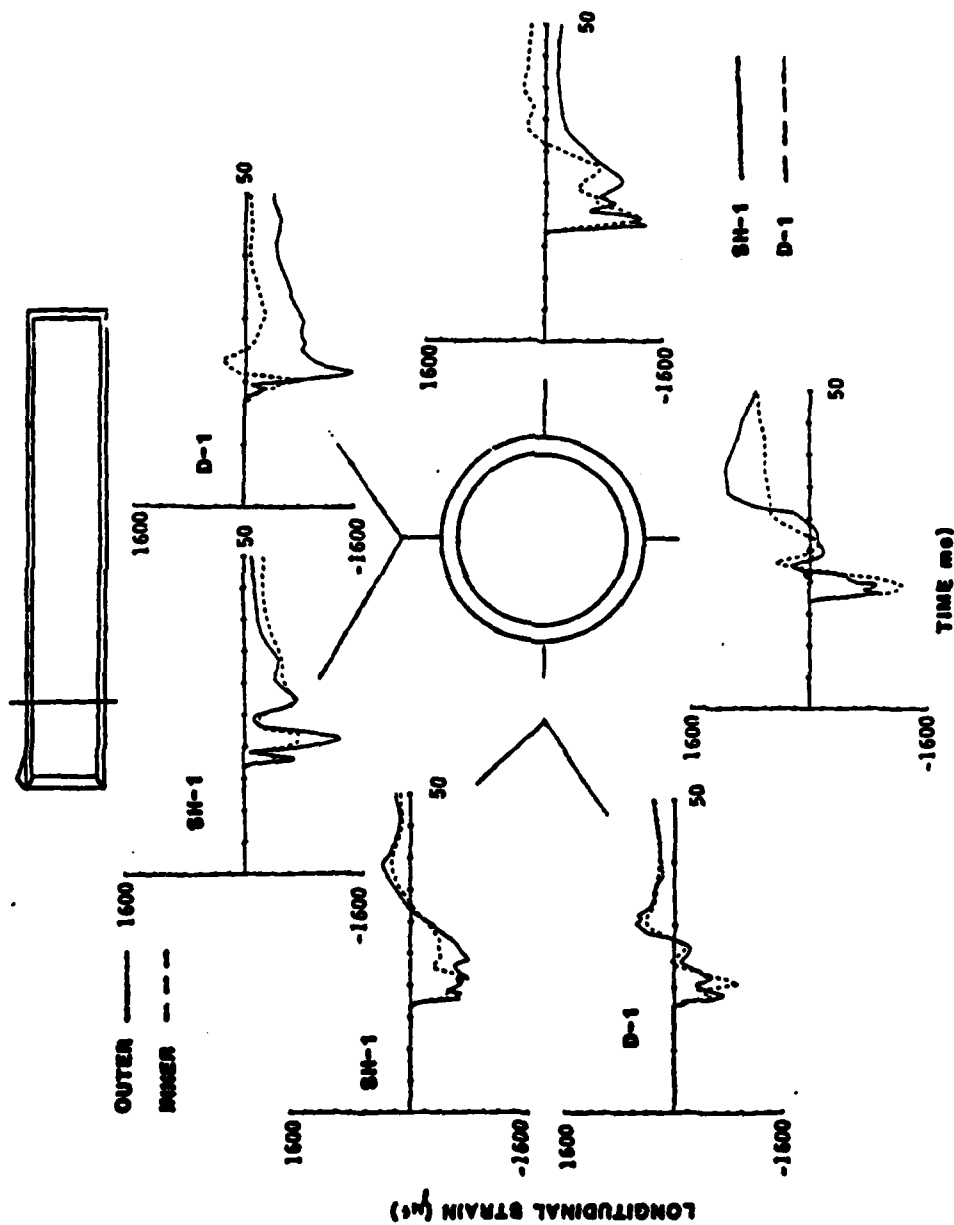
13

Figure 8. Closure base pan strain.

14

Figure 9. Longitudinal strain at 2 meters.

15

The overall agreement is very good between waveforms and magnitudes. Several differences are apparent due to the loading condition variation between the DABS and the HEST. The D-1 frontal airblast loading was greater at the bottom of the headwall than the top of the headwall and greater on the downstream side than the upstream side of the closure. The result was a bending moment seen in the strain data during the initial airblast loading compressive peak. The strain data displayed greater compression at the invert than the crown and greater compression at the downstream springline (due to the hinge area and the greater airblast pressure loading) than at the upstream springline. While this same bending moment occurs in the horizontal direction in SH-1 (influenced most by the presence of the hinge), the vertical moment is not seen in SH-1 due to the constant load distribution vertically on the face of the structure. These longitudinal strain comparisons also illustrate the common longitudinal modes of response: an initial compressive peak due to direct airblast loading, followed by relief and a vertical longitudinal bending which causes compression in the crown as the normal stress from airblast loading of the berm arrives and generates large shear stresses. These shear stresses act to slow the structural motions, and the normal stresses also induce the vertical longitudinal bending of the structure. The severity of the normal stress on the crown can also cause localized wall bending, which is seen clearly in the D-1 data but more moderately in the SH-1 data at this location. The final longitudinal response mode is seen at around 26 to 28 milliseconds as the drag-back shear stress in the forward region of the structure interacts with the resisting shear stress and the end wall support further aft to cause a smooth transient compressive strain pulse as the structure vertically bends.

Mid-structure longitudinal strains, shown in Figure 10, follow the trends seen in the more forward location. All the waveforms agree in shape and timing, but SH-1 shows more extreme strains due to the higher loading (except at the crown). The difference in strain at the crown between 20 and 25 ms is due to the vertical longitudinal bending in SH-1, which occurs farther back from the headworks than in D-1 and results in more compressive strains in the crown as the bending takes
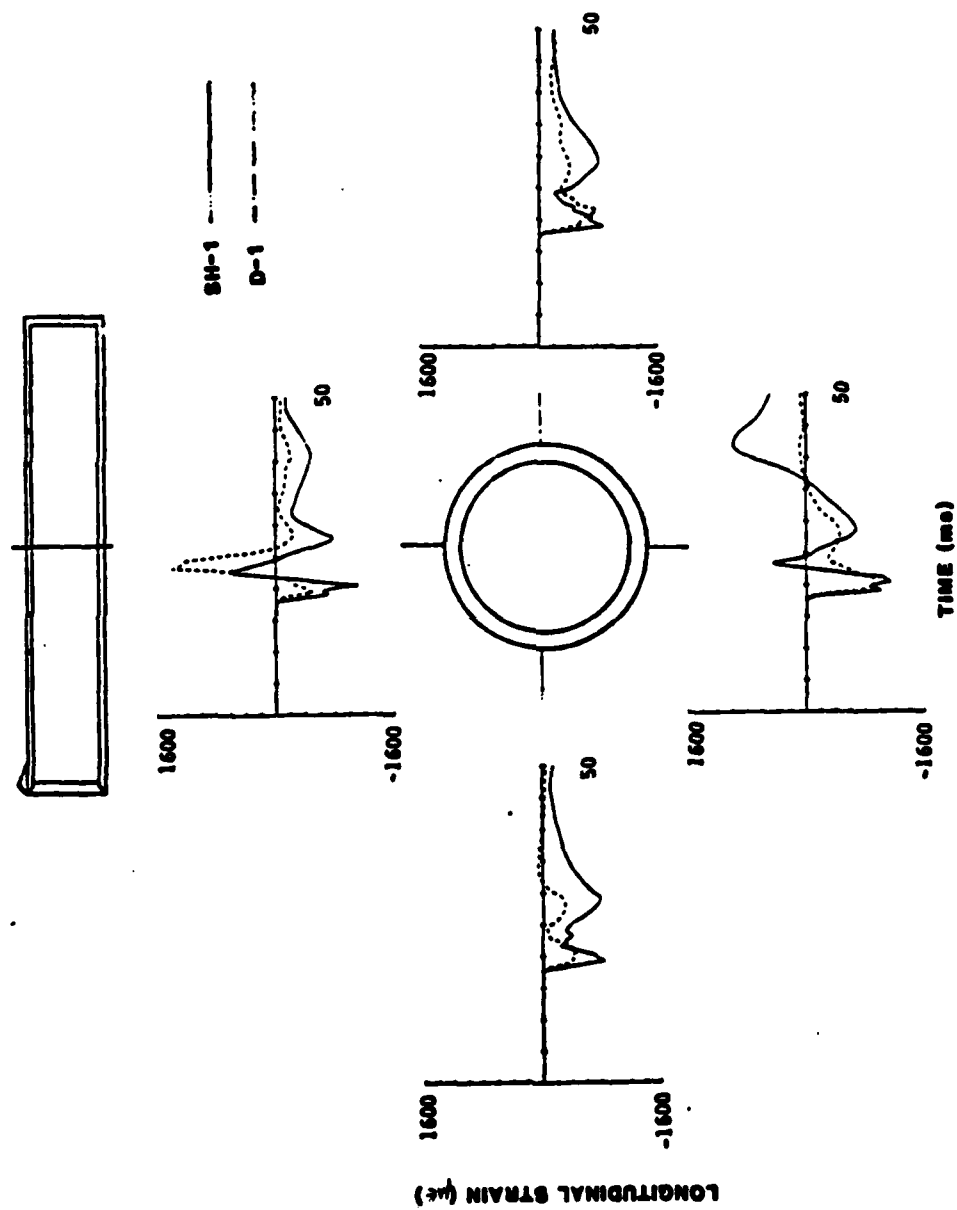
Figure 10. Mid-structure longitudinal strains.

17

place. This effect due to vertical longitudinal bending is seen in the invert strain data as well, where the tensile strains caused by the bending show up in SH-1 but are not as severe in D-1 data. The pronounced relief seen in both tests between 20 and 25 milliseconds is due to the fact that the normal stress and resultant shear stresses are acting to restrain the longitudinal motion of the forward portion of the structure while the aft portion of the structure is reaching peak longitudinal motions due to direct airblast loading. However, the major point of this comparison is that both tests continue to direct the identical response modes from the structure with slight changes due to the difference in loading in the two simulations.

Figure 11 compares the circumferential strains for D-1 and SH-1 test structures from data taken at the inner face and outer longitudinal rebar at each location in the cross-section. As mentioned earlier, the structural ovaling response consists of two positive ovaling phases (crown and invert move closer) with a relief in between. The relief between positive ovaling response peaks is more pronounced in D-1, when negative ovaling occurred at times between the positive ovaling responses. The initial ovaling phase was caused by the application of normal stress at the crown due to airblast pressure loading of the berm over the structure, while the relief was caused by the flow of the normal stress around to the springlines as it propagated vertically. Finally, the second positive phase occurred as the normal stress engulfed the structure and the vertical motion of the structure downward was halted due to the compaction of the cradle material beneath the invert. The second positive ovaling phase seems more severe due to the higher strain magnitudes, but the reduced concrete cross-section due to cracking of the concrete in the initial positive ovaling phase accounts for that exaggeration. Figure 11 illustrates all of these points, and once again the SH-1 response is generally greater due to the higher loading in the simulation. The springlines provide the closest match, while higher ovaling modes seem to be present at the crown in SH-1 and at the invert in D-1.

Shown in Figure 12, lateral strains on the inner and outer surfaces of the endwall are compared for D-1 and SH-1 at the center and the rim. Timing and shape of the waveforms agree very well in all cases, with SH-1 experiencing the higher strains, as expected. At the center,
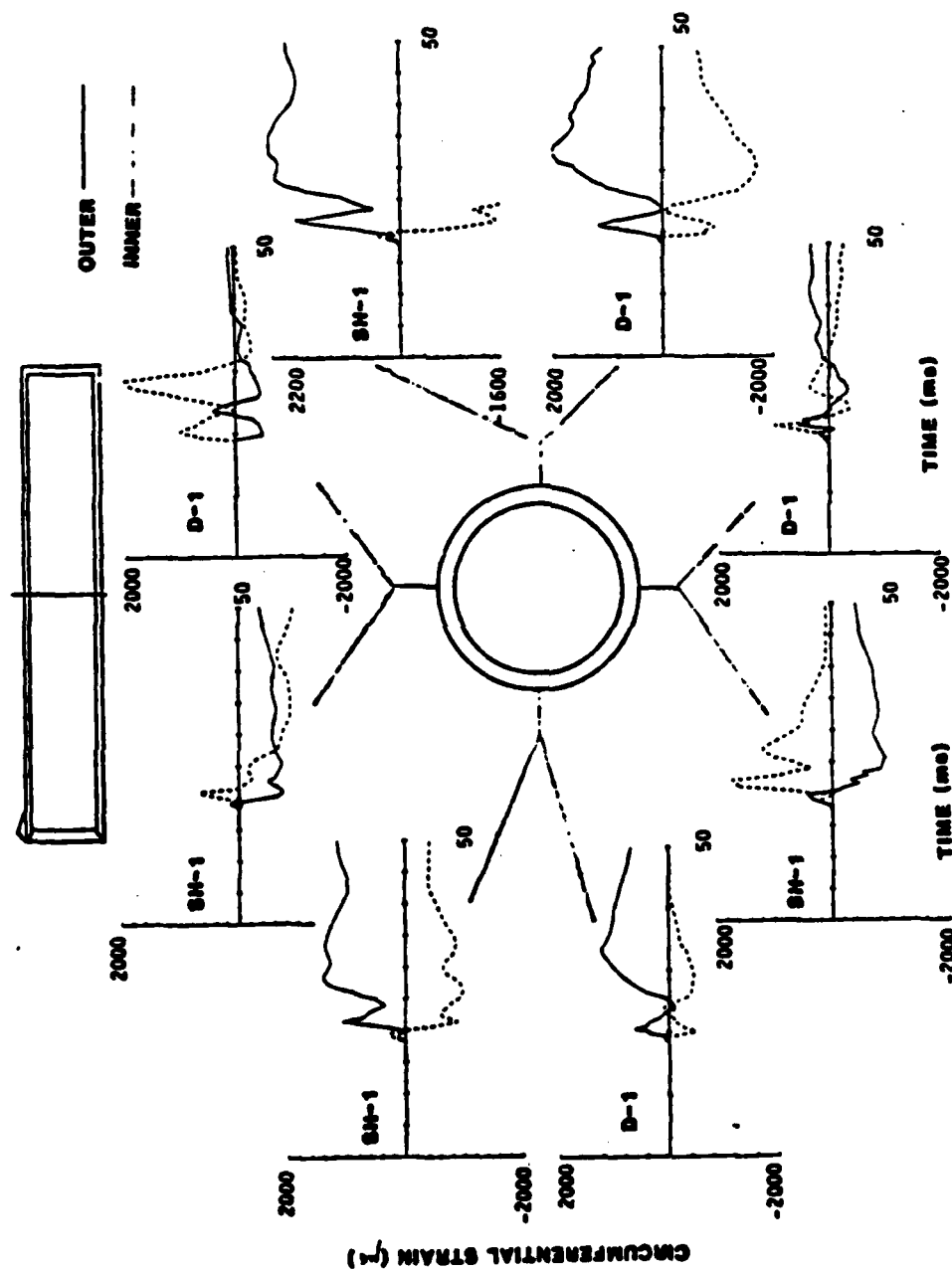
18

Figure 11. Mid-structure circumferential strains.
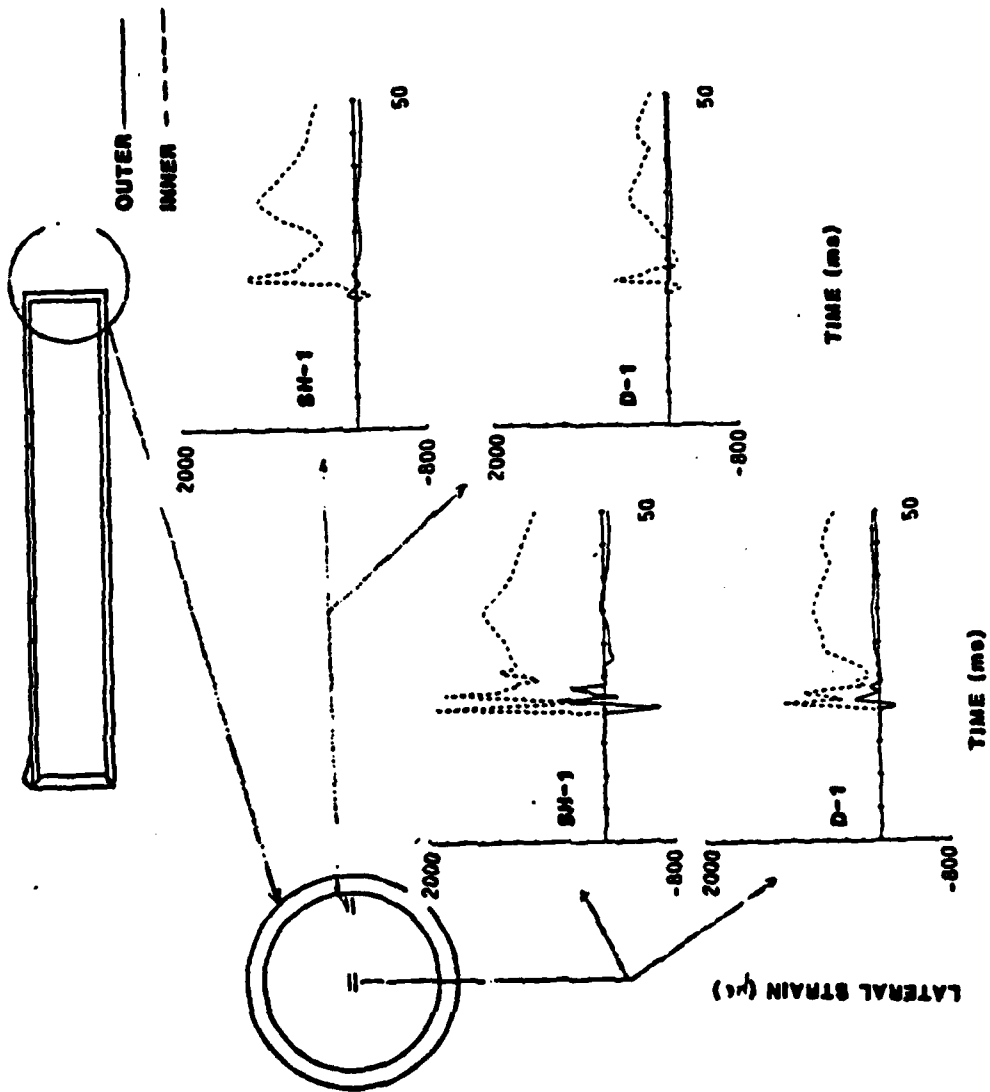
19

Figure 12.   End wall lateral strains.

20

the endwall dishing into the structure causes initial outer surface compression and inner surface tension. As the load increases, the endwall goes into overall section tension with the bending moment still evident in the data. The initial peak is due to structural displacement under direct airblast loading. The second peak is caused by the propagation of the vertical airblast-induced ground shock down through the berm, and the final long peak is due to the same cause as the second longitudinal strain and longitudinal velocity peaks seen throughout the SH-1 structure-secondary airblast peak loads on the face of the structure and drag-back shear stress acting in the frontal region of the structure. The same effects are seen at the rim, except that the outer strain gage is relieved of load due to edge effects near the outer corner of the structures, and thus that gage gives a very minor strain reading. The inner strains at the rim go into initial compression as the endwall dishes in, but then the load increases to cause overall section tension seen in the gage. The second peak, due to vertical airblast-induced ground shock, is not as isolated an event at the rim, and that peak is seen as a bump on the decreasing side of the initial peak. Given the complexity of the response of the endwall, the two tests agree very well in timing and shape, with the only discrepancy being the greater magnitudes in SH-1 strains due to the loading differences with D-1.

Strain data analysis, based on understanding of the loading condition differences and motion data, makes a very strong case for the abil ty of a HEST simulator to mimic the loading of a DABS when simulating a given blast environment.

CONCLUSION.

Comparisons between the D-1 test data and the SH-1 test data reveal that similar structural response modes were observed in both tests. The only differences stem from the difference in the airblast loading simulation in SH-1 compared to a D-1 standard, and that is a discrepancy which can be corrected with a refined HEST design and proper calibration of the HEST design. Using structural response as a yardstick, therefore, the less costly HEST simulator is as viable a choice in testing generic structure designs under anticipated airblast conditions as the more expensive DABS simulator.

SUMMARY

A Comparison of Nuclear Simulation Techniques on Generic MX Structures, by John F. Betz. Two separate 1/5 scale tests were run on a generic MX protective structure using different simulators to create a standard blast environment. Based on analysis of the structural data, the less expensive HEST simulator was as good a simulator as the more expensive DABS simulator.

A COMPARISON OF NUCLEAR SIMULATION TECHNIQUES ON
GENERIC MX STRUCTURES

ABSTRACT: A HEST (High Explosive Simulation Technique) is as good a
simulator of an airblast environment as a DABS (Dynamic Airblast Simula-
tor). A study performed on the results of two identical 1/5 scale pro-
tective structures when tested under matching environments produced by
each of the simulators revealed data which supports the viability of
the HEST simulator, which is less costly and was thought to be of less
fidelity than a DABS simulation. Structural response data, which is
used as a yardstick to compare simulators, shows identical response
modes are produced by the two simulators as arranged in the matching
tests.

E

ED

83